Co-published by
Institute of Fluid-Flow Machinery
Polish Academy of Sciences
Committee on Thermodynamics and Combustion
Polish Academy of Sciences

http://www.imp.gda.pl/archives-of-thermodynamics/

One-dimensional model of solid oxide fuel cell for advanced hybrid energy systems analysis

Julian Piotr Jędrzejewski[a,b*], Sebastian Lepszy[a], Sebastian Rulik[a]

[a]Silesian University of Technology, Faculty of Energy and Environmental Engineering, Konarskiego 18, 44-100 Gliwice, Poland
[b]Antea Polska S.A., Dulęby 5, 40-833 Katowice, Poland
*Corresponding author email: sebastian.lepszy@polsl.pl

Received: 02.11.2024; revised: 23.12.2025; accepted: 23.01.2026

Abstract

Growing demand for electricity and the intensification of the use of renewable energy sources create the need for the development of energy technologies, including hydrogen-based solutions. In the context of generating energy from hydrogen, fuel cells are characterised by particularly favourable operating parameters. The literature identifies several types of fuel cells, among which high-temperature solid oxide fuel cells (SOFCs) show significant application potential. This is related, among other factors, to the possibility of integrating these cells into hybrid energy systems (fuel cell − gas cycle − steam cycle) with various configurations and high energy efficiency. To determine the optimal structures of hybrid systems, detailed system analyses are essential, requiring accurate modelling of fuel cell characteristics. Depending on the objective of the analyses, the cell models may vary in complexity. This paper presents an advanced one-dimensional fuel cell model, enabling more realistic preliminary thermodynamic and economic analyses of hybrid systems. This model facilitates the assessment of efficiency, dimensions and exhaust media parameters. Furthermore, it allows for the verification of whether the cell parameters used in the analyses align with their practical implementation capabilities.

Keywords: Hybrid energy systems; SOFC; One-dimensional modelling; High-temperature fuel cell

Vol. 47(2026), No. 1, 113–123; doi: 10.24425/ather.2025.156859

Cite this manuscript as: Jędrzejewski, J.P., Lepszy, S., & Rulik, S. (2026). One-dimensional model of solid oxide fuel cell for advanced hybrid energy systems analysis. *Archives of Thermodynamics*, 47(1), 113–123.

1. Introduction

The increase in installed capacity in renewable energy sources, driven by the fight against global warming and the growing demand for electricity, is driving the development of energy storage technologies. One promising energy carrier which offers the possibility of long-term storage and zero-emission generation of electricity and heat is hydrogen. In the context of generating energy from hydrogen, fuel cells exhibit particularly favourable operating parameters. Fuel cells are electrochemical systems that convert the chemical energy from a fuel oxidation reaction directly into electricity and heat [1]. The literature identifies several types of fuel cells, including polymer electrolyte membrane fuel cells (PEM), alkaline fuel cells (AFC), phosphoric acid fuel cells (PAFC) and solid oxide fuel cells (SOFC) [2−4]. Among these, SOFCs show significant application potential, as evidenced by various review works, such as [5−7], just to name the most recent. Fuel cells of this type operate at very high temperatures – up to 1000°C – eliminating the need for precious-metal catalyst [2]. High-temperature SOFCs are also noted by their high electrical efficiency [1,8] reaching up to 49% [9]. In addition, SOFCs can be integrated into hybrid systems, achieving electrical efficiencies of up to 60% [10]. Numerous studies have explored cogeneration systems based on high-temperature SOFC. In [11], the authors analyse the economic feasibility of SOFC-based cogeneration systems for non-residential buildings, particularly supermarkets.

Nomenclature

A – channel area, m^2
c_p – specific heat at constant pressure, J/(kg K)
d – diameter or characteristic linear dimension, m
f – friction coefficient
FUF– fuel utilisation factor
$\dot{H}$ – physical enthalpy flow, W
I – current intensity, A
L – length, m
LHV– lower heating value, J/kg
$\dot{m}$ – mass flow rate, kg/s
N – power, W
Nu – Nusselt number
O – fluid-wetted perimeter of the channel, m
p – pressure, Pa
Pr – Prandtl number
$\dot{Q}$ – thermal energy flow, W
r – unit resistance, Ω/cm^2
R – resistance, Ω
Re – Reynolds number
t – temperature, °C
U – voltage, V
w – velocity, m/s

Greek symbols

α – heat transfer coefficient, W/(m^2 K)
Δ – change (drop or increase)
η – efficiency
λ – thermal conductivity coefficient, W/(m·K)
μ – dynamic viscosity coefficient, Pa·s
ν – kinematic viscosity coefficient, m^2/s
ρ – density, kg/m^3

Subscripts and Superscripts

a – air
el – electric
f – fuel
FC – fuel cell
H2 – hydrogen
i – inlet
l – laminar
lim – limit
o – outlet
s – series
t – turbulent
0 – no load

Abbreviations and Acronyms

CHP – combined heat and power
LSM – $La_{0.8}Sr_{0.2}MnO_{3-\delta}$ (perovskite-type oxide)
PEM – polymer electrolyte membrane fuel cell
SOEC – solid oxide electrolyser cell
SOFC – solid oxide fuel cell
YSZ – yttria stabilised zirconia
0D – zero-dimensional
1D – one-dimensional
2D – two-dimensional
3D – three-dimensional

While [12] presents designing and optimising a hybrid cogeneration system for off-grid applications, based on an SOFC as the primary energy source, integrated with hydrogen storage, a PEM fuel cell, and a battery, to enhance system flexibility, reduce investment costs, and extend SOFC lifetime by enabling steady-load operation. The authors of [13] aim to design and analyse a novel, carbon-free tri-generation system that utilises a combined SOFC and solid oxide electrolyser cell (SOEC) to produce hydrogen, electricity, and heat from natural gas, while enabling efficient CO_2 capture and decentralised energy supply. In [14], the authors provide a comprehensive review of fuel cell-based micro-combined-heat-and-power (micro-CHP) systems, focusing on their configurations, fuel processing methods, thermal management, and integration with other technologies like energy storage and renewable sources.

To determine the optimal structure of hybrid systems, detailed system analyses are necessary, requiring accurate modelling of fuel cell characteristics.

According to [15,16], there are three core types of approaches of SOFC modelling based on how much physical knowledge is embedded in the model:

- physical (white-box) models, which are based purely on physics and chemistry laws;
- black-box models, which are based on empirical data and machine learning;
- grey-box (hybrid) models, which are the combination of physical modelling and data-driven components.

Physical models are used for design, simulation and diagnostics, while black-box models are used for control and fault detection. The grey-box models are used for real-time modelling and diagnostics [15]. In this paper, the authors focused on physical models.

Physical models are fully physics-based models, derived from electrochemistry, thermodynamics, heat and mass transfer, as well as electrical conduction laws [16]. These models are characterised by high interpretability and accuracy, and are typically represented by partial differential equations (PDEs) or ordinary differential equations (ODEs). These models require detailed material and geometry data.

Physical models are divided into:

- multi-dimensional models, which are used for modelling from full spatial detail to system-level specifications [15,16];
- electrochemical impedance spectroscopy (EIS) based equivalent circuit models, which use impedance spectroscopy for parameter estimation and fault diagnosis [15].

Dimensional models can be divided into:

- Three-dimensional (3D) models are the most detailed and accurate, capturing full spatial variations in all directions. They are used to analyse local behaviours, such as temperature gradients, current density distribution and fuel utilisation. These models are computationally intensive and best suited for design optimisation and high-fidelity simulations [15,16].

- Two-dimensional (2D) models simplify geometry by neglecting one spatial dimension. They are commonly applied to symmetric or repetitive designs (e.g. planar or tubular cells). These models are useful for analysing cross-sectional behaviour and allow a good trade-off between accuracy and computational efficiency [15].
- One-dimensional (1D) models assume variation along a single direction – typically the gas flow direction. Effects like concentration and ohmic losses in neglected dimensions are often handled using empirical corrections or averaged parameters. These models are suitable for evaluating overall cell performance, dynamic response, and simplified control or hybrid system studies [15].
- Zero-dimensional (0D) models treat the entire SOFC or system as a lumped unit with spatially averaged parameters. These models are used in system-level simulations, such as SOFC–gas turbine hybrids or CHP systems. While they cannot capture internal cell phenomena, they are ideal for rapid performance estimation, control and parametric/system-level optimisation [15].

In [17], the authors present a 1D dynamic model of SOFC developed to enhance real-time predictions of temperature and pressure variations along the cell, outperforming existing 0D models. The model demonstrates that activation overpotentials are significant and that optimising gas channel configurations can reduce the required pumping power.

In [18], the authors present two computational models for predicting the electrical performance of a tubular SOFC designed by Siemens Westinghouse Corporation. The first model employs simplifying assumptions for activation and concentration polarisations to obtain an analytical solution, while the second model allows these polarisations to vary with current density and solves the equations numerically. Both models show good agreement with experimental results, making the simpler analytical model useful for predicting cell performance based on dimensions and aiding in cost-performance analysis.

The paper [19] compares 0D and 1D modelling techniques for predicting the performance of tubular SOFCs. It finds that, while 0D models tend to overestimate voltage, power and temperature, 1D models offer more accurate local current density predictions along the cell. The study underscores the importance of discretisation in enhancing model accuracy and demonstrates that temperature distribution is critical for optimising SOFC design and performance.

The work [20] specifically examines mathematical modelling of SOFCs, focusing on both tubular and planar configurations. It discusses various factors, including mass, energy and momentum transfer, diffusion through porous media, electrochemical reactions and polarisation losses, while also comparing the effects of different fuels on SOFC performance. Additionally, the review highlights novel modelling approaches, including data-driven techniques like artificial neural networks, and suggests areas for further research to enhance SOFC models and improve predictions of fuel cell behaviour.

Paper [21] presents a detailed 1D, axial-symmetric model of a tubular SOFC, incorporating advanced descriptions of electrochemical reactions, internal reforming kinetics, and thermodynamic balances to predict temperature, pressure and composition profiles along the cell. A comprehensive case study and sensitivity analysis demonstrate how key design and operational parameters impact performance, challenging common simplifications in existing SOFC models.

The study presented in [22] develops a fast, high-fidelity 1D thermodynamic model for SOFC stacks that uses experimental data to identify optimal operating conditions and efficiency-performance trade-offs without requiring costly simulations or experiments.

The literature also contains numerous papers addressing 2D models [23,24] as well as 3D models [25,26]. The study presented in [27] introduces a computationally efficient 3D multiphysics model using backpropagation neural networks to optimise the structural design of large-scale SOFC stacks and towers, improving flow uniformity, temperature distribution, and overall performance.

Paper [28] presents a detailed 3D numerical simulation of a 1 kW hydrogen-fuelled planar SOFC stack to investigate internal thermal conditions and heat transfer mechanisms under realistic operating conditions and actual geometry. The study reveals that air flow and heat capacity dominate the temperature distribution and gradients, with air advection and interconnect conduction being the key heat transfer pathways, highlighting the importance of thermal management strategies for reducing thermal stress and enhancing stack reliability.

Unlike the study presented in [28], this work focuses on simpler system models that require less computational memory and time. System models simulate the overall behaviour of the cell within a complete power generation system, rather than resolving all the internal physical and chemical processes in fine detail. These models are preferably used when multiple variants of a case (numbering in hundreds) have to be analysed [17].

The primary objective of this study is to develop an analytical model that utilises available current-voltage (*I-V*) characteristics to estimate both the geometric sizing of a solid oxide fuel cell and the thermodynamic properties of the electrochemical reaction products. Rather than aiming to replicate the detailed internal electrochemical and transport phenomena typically captured in high-resolution one-dimensional models, this work focuses on constructing a phenomenological framework that balances physical realism with numerical simplicity. The model is designed specifically for integration into broader hybrid energy systems − such as configurations combining SOFCs with air turbines − where system-level optimisation and computational efficiency are critical.

The proposed approach prioritises scalability and computational speed over high-fidelity resolution, enabling its application in iterative design processes, parametric analyses and techno-economic evaluations. By introducing justified simplifications that preserve core predictive capabilities, the model facilitates significant reductions in computational demand, making it practical for early-stage design and decision-making workflows.

Key outputs of the model include the specific power density of the fuel cell, the active electrochemical surface area, internal energy losses and the thermodynamic characteristics of exhaust

gases. These parameters provide a foundation for subsequent cost estimation algorithms and system-level performance evaluations. Ultimately, the model supports the optimisation of hybrid configurations with respect to both energy efficiency and economic performance, offering a valuable tool for the development of advanced, high-efficiency energy systems.

2. Fuel cell model

The analyses employed a 1D model of tubular SOFC fuel cells. The presented model utilises current-voltage characteristics based on experimental data or physical models developed by other researchers, in such a way that it enables the determination of the size of the modelled fuel cell and the output parameters of the products of electrochemical reactions occurring within the cell. The model's calculation algorithm divides the fuel cell into elementary ring-shaped sections, for which the outlet parameters are computed based on the input parameters. Additionally, the algorithm assumes that there is no voltage drop during current flow along the electrodes. The omission of voltage drops along the electrodes − resulting from electronic and ionic resistances within the electrode materials − can lead to an overestimation of both the efficiency and power output predicted by the model. While these internal losses may be negligible in small-scale fuel cells or under moderate current densities, they become increasingly significant in larger systems or during high-current operation. Under such conditions, the associated non-uniformities in potential and temperature distributions can impact local reaction rates and overall system performance. Nonetheless, the level of accuracy retained is considered sufficient for the intended application of the model, which prioritises computational efficiency and system-level analysis over detailed intra-cell resolution.

To determine the operating parameters of the fuel cell, the characteristic proposed by Milewski [29] was utilised. The cell for which the characteristics are given has the main layers as follows:

- first anode layer made of Ni + YSZ (yttria stabilised zirconia),
- second anode layer made of Ni + YSZ,
- electrolyte layer made of YSZ,
- second cathode layer made of LSM ($La_{0.8}Sr_{0.2}MnO_{3-\delta}$) + YSZ,
- first cathode layer made of LSM.

The current-voltage characteristic has been compared with actual experimental data [29]. The literature includes publications presenting current-voltage characteristics of SOFCs based on the same electrode and electrolyte materials [30−33]. The characteristic used in this study is consistent with the results reported in the aforementioned works.

To simplify the calculations, linearised current-voltage characteristics (Fig. 1) for three operating temperatures were used as a data source for the substitute fuel cell model.

The linearisation of the current-voltage characteristic constitutes a fundamental simplification of the inherently nonlinear electrochemical behaviour of solid oxide fuel cells (SOFCs). In practice, the cell voltage is governed by a combination of activation, ohmic and concentration overpotentials, all of which exhibit increasingly nonlinear behaviour as current density rises. By

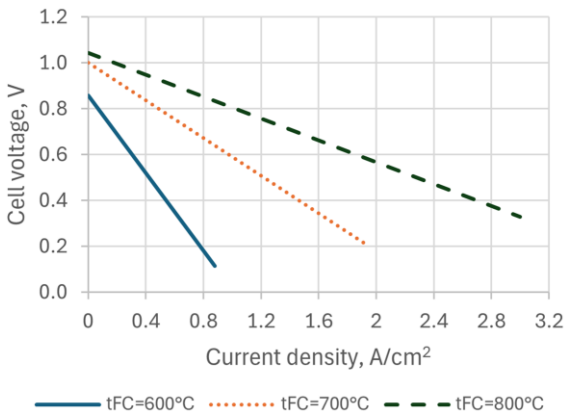

Fig. 1. Simplified current-voltage characteristic of the fuel cell for three cell operating temperatures.

adopting a linear approximation of the current-voltage relationship, the model may inadequately represent these phenomena, potentially resulting in either underestimation or overestimation of cell voltage, depending on the specific operating conditions. This limitation becomes particularly pronounced under extreme operational scenarios − such as high load demand − where nonlinear effects dominate the electrochemical response. Nevertheless, the proposed linear approximation demonstrates satisfactory agreement with experimental data, providing an acceptable level of accuracy for the model's intended applications, which prioritise computational efficiency and system-level integration.

Linearisation of the fuel cell characteristics enables the use of an electrical model of an elementary fuel cell represented as a voltage source in series with a resistance (Fig. 2).

Based on the fuel cell model and the linearised characteristics, the relationship between the unit series resistance and no-load voltage as a function of temperature was established. This relationship is expressed by the following formulas:

$$r_s = 36.374 \exp(-0.006t), \tag{1}$$

$$U_0 = 0.00093t + 0.3, \tag{2}$$

where: r_s – unit series resistance, U_0 – no-load cell voltage, t – fuel cell temperature.

The 1D model uses the principle of conservation of momentum to determine the pressure drop during the flow of agents. In these calculations, it is assumed that the velocity and density of the agent remain constant within the elementary section and are equal to the outlet values from the previous element. Consequently, the pressure losses during the flow of agents are calculated using the Darcy-Weisbach equation:

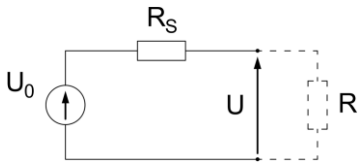

Fig. 2. Simplified model of a fuel cell.

$$\Delta p = f\frac{\rho w^2}{2}\frac{O}{4A}\Delta L, \tag{3}$$

where: Δp – pressure loss, f – friction coefficient, ρ – density of an agent, w – velocity of an agent, O – agent-wetted perimeter of the channel, A – channel area, ΔL – section length.

The friction coefficient was determined using the equation proposed by Churchill [34], which is applicable for laminar, turbulent and transitional flow for smooth pipes:

$$f = 2\left[\left(\frac{8}{\mathrm{Re}}\right)^{12} + \frac{1}{(A+B)^{\frac{3}{2}}}\right]^{\frac{1}{12}}, \tag{4}$$

$$A = \left[2.457\ln\left(\frac{1}{\frac{7}{\mathrm{Re}}+0.27\frac{O}{d}}\right)\right]^{16}, \tag{5}$$

$$B = \left(\frac{37.53}{\mathrm{Re}}\right)^{16}, \tag{6}$$

where: Re – Reynolds number, d – diameter or characteristic linear dimension.

Dynamic viscosity was determined using the CoolProp library [35]. Kinematic viscosity was determined according to the formula

$$\nu = \frac{\mu}{\rho}, \tag{7}$$

where μ is the dynamic viscosity coefficient.

The Reynolds number was calculated using the formula

$$\mathrm{Re} = \frac{w\cdot d}{\nu}. \tag{8}$$

The Prandtl number was calculated using the formula

$$\mathrm{Pr} = \frac{\mu c_p}{\lambda}, \tag{9}$$

where: c_p – specific heat at constant pressure, λ – thermal conductivity coefficient.

The thermal conductivity coefficient and specific heat were also determined using the CoolProp library.

Dynamic viscosity and thermal conductivity were determined as functions of temperature and partial pressure.

For the elementary section of the fuel cell, the energy balance was formulated using equations in the following form:

$$\dot{H}_{ai} + \dot{H}_{fi} + \dot{Q}_{\mathrm{FC}} = \dot{H}_{ao} + \dot{H}_{fo} + N_{\mathrm{elFC}}, \tag{10}$$

$$\dot{Q}_{\mathrm{FC}} = (1-\eta_{\mathrm{elFC}})\Delta\dot{m}_{\mathrm{H2}}\mathrm{LHV}_{\mathrm{H2}}, \tag{11}$$

$$N_{\mathrm{elFC}} = \eta_{\mathrm{elFC}}\Delta\dot{m}_{\mathrm{H2}}\mathrm{LHV}_{\mathrm{H2}}, \tag{12}$$

where: $\dot{H}_{ai}$ – physical enthalpy flow of air at the inlet, $\dot{H}_{fi}$ – physical enthalpy flow of fuel at the inlet, $\dot{Q}_{\mathrm{FC}}$ – thermal energy flow from the chemical reaction of hydrogen and oxygen, $\dot{H}_{ao}$ – physical enthalpy flow of air at the outlet, $\dot{H}_{fo}$ – physical enthalpy flow of fuel at the outlet, N_{elFC} – electrical energy from the reaction of hydrogen and oxygen, η_{elFC} – electrical efficiency of the fuel cell, $\Delta\dot{m}_{\mathrm{H2}}$ – mass flow of hydrogen reacting with oxygen, and $\mathrm{LHV}_{\mathrm{H2}}$ – lower heating value of hydrogen.

Physical enthalpy is also determined using the CoolProp library. The input data required to calculate the physical enthalpy of a gas mixture are the mass composition of the gas, its temperature and pressure, and the reference temperature.

It was assumed that the primary mechanism influencing heat transfer in the elementary element is heat convection. This assumption simplifies the calculations while ensuring a balanced temperature in the modelled fuel cell element.

The key parameter for determining the amount of heat flowing from the fuel cell to the surrounding medium is the heat transfer coefficient. Its value was calculated based on the friction coefficient. The Nusselt number developed by Gnieliński (after [36]) was used to determine the heat transfer coefficient:

$$\mathrm{Nu}_t = \frac{\frac{f}{8}\mathrm{Pr}(\mathrm{Re}-1000)}{1+12.7\sqrt{\frac{f}{8}}\left(\mathrm{Pr}^{\frac{2}{3}}-1\right)}, \tag{13}$$

$$\mathrm{Nu}_l = \left\{3.66^3 + 0.7^3 + \left[1.615\left(\mathrm{RePr}\frac{d}{L}\right)^{\frac{1}{3}} - 0.7\right]^3 + \left(\frac{2}{1+22\mathrm{Pr}}\right)^{\frac{1}{6}}\left(\mathrm{RePr}\frac{d}{L}\right)^{\frac{1}{2}}\right\}, \tag{14}$$

$$\mathrm{Nu} = \mathrm{Nu}_{l,2300} + \frac{(\mathrm{Nu}_{t,4000}-\mathrm{Nu}_{l,2300})(\mathrm{Re}-2300)}{4000-2300}, \tag{15}$$

where: Nu_t – Nusselt number for turbulent flow, Nu_l – Nusselt number for laminar flow, $\mathrm{Nu}_{l,2300}$ – Nusselt number for laminar flow at Re = 2300, $\mathrm{Nu}_{t,4000}$ – Nusselt number for turbulent flow at Re = 4000, d – channel diameter, L – channel length.

The heat transfer coefficient was determined based on the calculated Nusselt number:

$$\alpha = \frac{\mathrm{Nu}\lambda}{d}, \tag{16}$$

where: α – heat transfer coefficient, d – characteristic linear dimension.

The presented model has been implemented in the SciLab environment. The model's results were obtained by solving the energy balance equations using an iterative method.

The main element determining the parameters of the fuel cell in the proposed model is its current-voltage characteristics. This approach ensures an accurate representation of the behaviour of real fuel cells across different scales. Modelling other types of cells with different designs (e.g. planar cells) requires significant changes in heat flow modelling, and obtaining reliable results in such cases necessitates three-dimensional analyses, which are more demanding in terms of model detail and computation time.

Modelling other flow directions is possible, but of limited relevance from the standpoint of the resulting exhaust gas temperatures and their potential for generating additional electrical energy in gas-based systems. Modelling cells made of other materials essentially reduces to changing the current-voltage characteristics of the cells used in the model.

3. Input parameters for analysis

In the modelling process, it was assumed that the fuel for the cell is hydrogen, comprising 95% by volume. Additionally, the fuel contains 4% nitrogen and 1% water vapour by volume. The fuel temperature is set at 20°C, and its pressure is equal to 1 bar(a). These values are based on the assumption that the model will be used for the analysis of a combined system with a gas turbine, where the fuel cell operates at a pressure close to the ambient pressure.

For the fuel cell, the air was assumed to have the following molar composition: nitrogen 78.1%, argon 0.9% and oxygen 21.0%. The analysis considered a high initial air temperature to enable the cell to start operating. The air pressure was maintained at 1 bar(a), with an air flow rate of 1 kg/s. The fuel flow rate was determined based on the assumed excess air coefficient λ. This assumption was made to decouple the model from the system scale.

One of the primary operating parameters of a stack, or multiple fuel cell elements connected in parallel, is the operating voltage of individual cells and the entire assembly. Theoretically, this voltage can range from 0 to U_{MAX}, depending on the operating temperature and the concentration of components, specifically hydrogen and oxygen. Due to simplifications in the form of linearisation of fuel cell characteristics, the range of operating voltage has been limited to between 0.2 V and 0.8 V.

Parametric calculations were performed assuming five variables for calculations:

- air velocity at the inlet to the cell, w_a (5–15 m/s);
- cell operating voltage, U (0.2–0.8 V);
- fuel utilisation limit factor, FUF_{lim} (0.6–0.8);
- excess air coefficient, λ (2.0–3.0);
- air temperature at the inlet to the cell, t_a (500–600°C).

The developed algorithm also provides error codes that indicate the following events:

- too many iterations of a given case (for the number of iterations exceeding 3000),
- fuel cell temperature exceeded 1000°C,
- the value of hydrogen used for at least one of the iterations is negative,
- the cross-sectional diameter of the cell channel is smaller than 5 mm,
- the fuel pressure drop exceeded 200 hPa,
- the air pressure drop exceeded 200 hPa.

The operational limitations embedded in the model's error-handling routine serve a dual purpose: they ensure numerical stability during simulations and help maintain the physical plausibility of results. If any of the predefined error conditions are encountered − such as violations of thermodynamic or electrochemical constraints − the algorithm automatically excludes the corresponding input set by returning an error code and terminating that specific computation. As a result, the range of output results presented is narrower than the full set of initially simulated conditions. While this approach enhances the reliability of the simulation by filtering out infeasible operating points, it also restricts the model's capacity to explore the full spectrum of scenarios encountered in practical SOFC-based hybrid systems, particularly near operational boundaries. Despite these constraints, the adopted simplifications are justified within the context of the model's intended application: early-stage design exploration, performance assessment and parametric analysis, where computational efficiency and simulation stability take precedence.

4. Results and discussion

The authors do not aim to model the fuel cell itself in detail, but rather to develop an analytical model of the cell that can subsequently be integrated into a hybrid system model – such as one in which the fuel cell operates in conjunction with an air turbine – to maximise electricity production within the analysed system. The outputs of the developed model include parameters such as specific power, properties of exhaust products and fuel cell active surface area. These parameters will, in the future, serve as a foundation for extending the model with an algorithm for calculating the cost of the fuel cell and the entire hybrid system, as well as for optimising the system in terms of both energy efficiency and economic performance. Results associated with error codes have been excluded from the analysis.

4.1. Unit power of the fuel cell as a function of the fuel cell operating voltage

Figure 3 shows the unit power of the fuel cell as a function of the cell operating voltage for various values of temperature and air velocity at the inlet to the fuel cell.

Parametric calculations were performed for voltages ranging from 0.2 V to 0.8 V, but the possible operating range of the cell is much narrower. For low voltages, the cell reached a temperature above 1000°C, which could result in its melting. This results from the low electrical efficiency of the cell for low voltages. The lower the electrical efficiency of the cell, the higher the amount of heat generated during the electrochemical reaction occurring in the cell, which results from Eq. (11). It should be noted that the higher the air temperature at the inlet to the cell, the higher the cell temperature for a larger range of low voltages. This can be explained directly from the energy balance of the cell (Eq. (10)), because the higher the enthalpy of the substrates, the faster the cell heats up to a given temperature. On the other hand, however, with an increase in the air temperature at the inlet to the fuel cell, the unit power obtained in the fuel cell increases, which results from Fig. 1 and Eq. (2).

Figure 3 clearly shows three groups of curves presenting the results for three given air temperatures at the inlet to the cell, i.e. 500°C, 550°C and 600°C – the higher the temperature, the higher the unit power obtained by the cell. This is related to an increase in the unit current intensity with an increase in the cell temperature (Fig. 1). In addition, the graph presented in Fig. 3

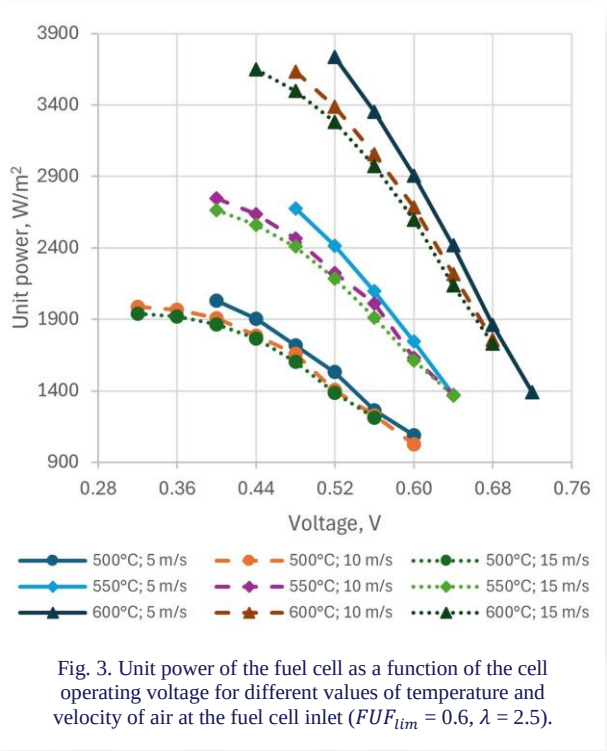

Fig. 3. Unit power of the fuel cell as a function of the cell operating voltage for different values of temperature and velocity of air at the fuel cell inlet (FUF_{lim} = 0.6, λ = 2.5).

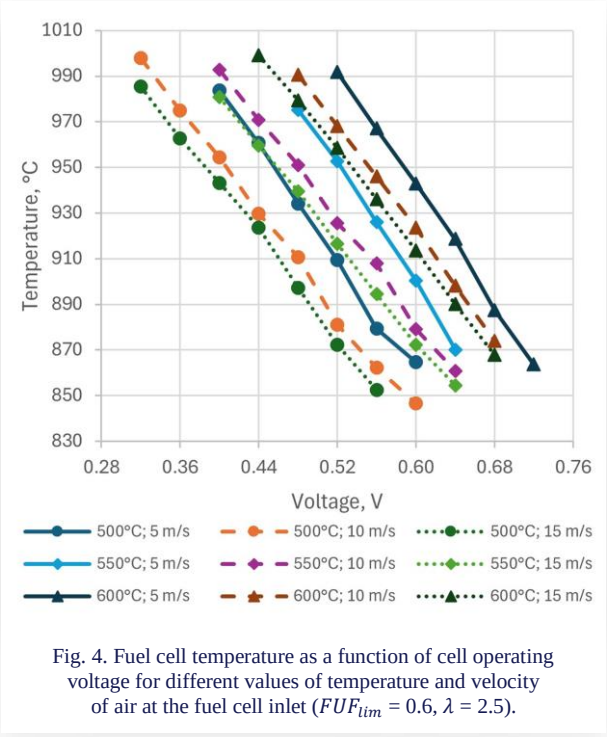

Fig. 4. Fuel cell temperature as a function of cell operating voltage for different values of temperature and velocity of air at the fuel cell inlet (FUF_{lim} = 0.6, λ = 2.5).

shows that the unit power of the fuel cell decreases with an increase in voltage, because the higher the voltage, the amount of fuel used per unit of the cell surface area decreases.

Another issue is the effect of the air velocity at the inlet to the cell on the unit power obtained in the cell. It is clearly visible that for each of the three temperature groups discussed above, the highest unit power values are obtained at the lowest values of inlet air velocity, i.e. 5 m/s. With the increase in this velocity, the results obtained for the individual voltages decrease slightly, and the possible range of the cell's operation shifts to higher voltages. Here comes the issue of the results obtained for the upper voltage range, for which the fuel pressure drop exceeded 200 hPa. The obtained fuel pressure drop results from the model assumptions and the efficiency of the fuel cells. One of the model input data is the value of the FUF. The model performs calculations until the set limit value FUF_{lim} is obtained. As mentioned earlier, the higher the voltage, the lower the fuel utilisation per unit of cell surface area, so to obtain the required FUF_{lim}, the cell surface area increases (the cell lengthens), which directly affects the increase in the fuel pressure drop at flow that results from Eq. (3).

4.2. Fuel cell temperature as a function of the fuel cell operating voltage

Figure 4 shows a graph of the fuel cell temperature as a function of the cell operating voltage for different values of temperature and velocity of air at the inlet to the cell. The graph clearly shows that the fuel cell temperature decreases with an increase in voltage. This results from the fact that the amount of fuel used per unit area decreases with an increase in the cell operating voltage (the unit fuel utilisation factor decreases). Also, the electrical efficiency of the fuel cell increases with an increase in the cell operating voltage, which means that less heat is released from the electrochemical reaction taking place in the cell (Eq. (11)). The graph also shows that as the air temperature at the inlet to the fuel cell increases, the cell operating range shifts to higher voltages. This results from the increase in electrical efficiency of the cell and the decrease in the amount of hydrogen reacted per unit area of the cell.

4.3. Fuel temperature at the outlet of the fuel cell as a function of the fuel cell operating voltage

Figure 5 shows a graph of the fuel temperature at the outlet of the fuel cell as a function of the fuel cell operating voltage for different values of temperature and velocity of air at the inlet to the fuel cell. The graph clearly shows that the fuel temperature at the outlet of the fuel cell decreases as the cell operating voltage increases. In addition, the graph shows three groups of curves characterised by the same air velocity at the inlet to the cell. For the lowest analysed air velocity at the inlet to the cell equal to 5 m/s, the lowest values of fuel temperature at the outlet of the fuel cell were obtained for the given values of air temperature at the inlet to the fuel cell and cell operating voltage. These values increased with the increase of air velocity at the inlet to the fuel cell and reached maximum values for the highest analysed velocity equal to 15 m/s. For each group discussed, one can observe the dependence of the increase in the fuel temperature at the outlet of the fuel cell on the increase in the air temperature at the inlet to the fuel cell, which, as mentioned above, results directly from the fuel cell balance equation (Eq. (10)). In addition, the graph (Fig. 5) shows that, among others, for the lowest air velocity at the inlet to the cell (5 m/s) and the air temperature at the inlet to the cell equal to 500°C and 600°C, a local minimum occurs, after which the fuel temperature rises as the cell operating voltage increases. With an increase in the cell operating voltage, the amount of heat delivered to the fuel and air

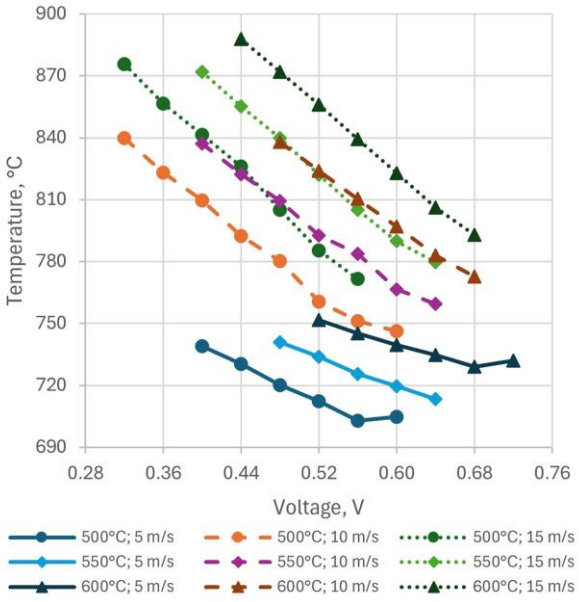

Fig. 5. Fuel temperature at the outlet of the fuel cell as a function of the cell operating voltage for different values of temperature and velocity of air at the inlet to the cell (FUF_{lim} = 0.6, λ = 2.5).

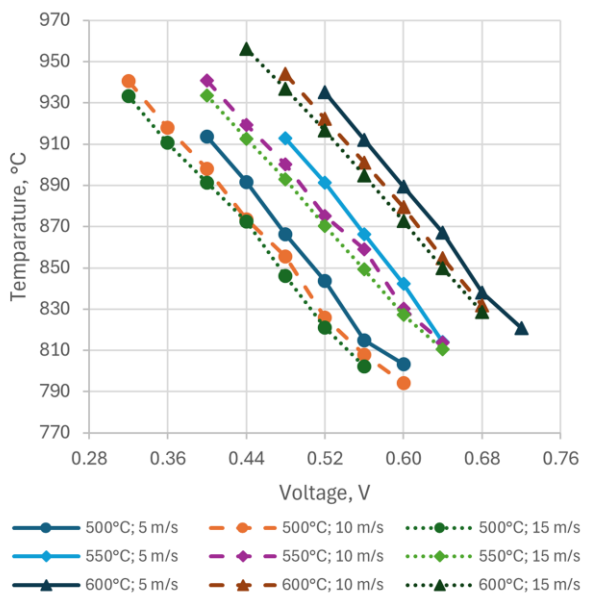

Fig. 6. Air temperature at the outlet of the fuel cell as a function of the fuel cell operating voltage for different values of temperature and velocity of air at the inlet to the cell (FUF_{lim} = 0.6, λ = 2.5).

decreases, but the decrease in this heat slows down from a certain limiting moment. At the same time, the temperature difference between the air and the fuel decreases because as the voltage increases, the cell lengthens. As a result, for low voltages, the decrease in the amount of heat with the increase in voltage prevails, while for higher voltages, the decrease in the temperature difference between the air and the fuel begins to be important. For a temperature of 500°C, the trend changes at a voltage of around 0.56 V, while for a temperature of 600°C, the trend changes at a voltage of approximately 0.68 V.

4.4. Air temperature at the outlet of the fuel cell as a function of the fuel cell operating voltage

Similar dependencies can be seen in the graph showing air temperature at the outlet of the fuel cell as a function of the cell operating voltage for different values of air temperature and velocity at the inlet to the cell (Fig. 6), i.e. as the cell operating voltage increases, the air temperature at the outlet of the fuel cell decreases. However, in this graph, the curves are grouped depending on the air temperature at the inlet to the fuel cell. Thus, the lowest values of the air temperature at the outlet of the fuel cell for the set values of air velocity at the inlet to the fuel cell and fuel cell operating voltage were obtained for the lowest set value of air temperature at the inlet to the fuel cell, i.e. 500°C. The air temperature at the outlet of the fuel cell increased with the increase of air temperature at the inlet to the fuel cell and obtained maximum values for the temperature of 600°C. As aforementioned, this follows directly from the cell balance equation (Eq. (10)). In addition, for individual groups, a relationship can be found between the drop in air temperature at the outlet of the fuel cell and the increase in air velocity at the inlet to the cell. This is due to the shorter contact time of the air with the hot fuel cell for higher air velocities.

4.5. Fuel pressure drop as a function of the fuel cell operating voltage

Figure 7 presents a graph illustrating the relationship between fuel pressure drop and fuel cell operating voltage for different air temperatures and velocities at the inlet to the fuel cell. The graph clearly shows that the fuel pressure drop increases with increasing voltage. As mentioned earlier, the described phenomenon results primarily from the model assumptions and specific properties of fuel cells. One of the key input parameters of the

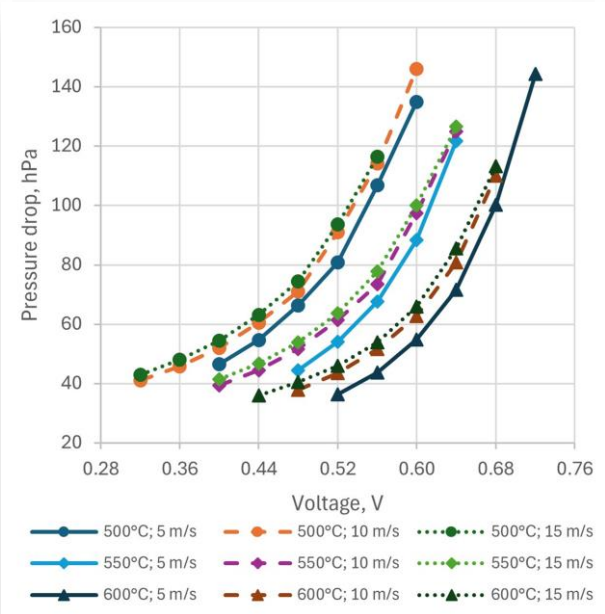

Fig. 7. Fuel pressure drop during flow through the fuel cell as a function of the fuel cell operating voltage for different values of temperature and velocity of air at the inlet to the fuel cell (FUF_{lim} = 0.6, λ = 2.5).

model is the FUF_{lim}. Calculations in the model are continued until the set limit value of the FUF_{lim} is reached. Higher voltage results in reduced fuel utilisation per unit of cell surface area. In order to achieve the required value FUF_{lim}, it is necessary to increase the cell surface area (by extending it), which directly affects an increase in the fuel pressure drop as it flows through the fuel cell (Eq. (3)).

The pressure drop value is also related to the temperature of the flowing gas, i.e. the higher the temperature, for a given voltage, the higher the unit current intensity in the fuel cell, according to Fig. 1. In turn, the higher the unit current intensity, the smaller the required fuel cell surface area to obtain the assumed FUF_{lim}; the cell is shorter, so the pressure drop associated with linear losses during flow through the channel is lower. The above relationship is evident from the graph, i.e. the decrease in fuel pressure losses during flow through the fuel cell with the increase in air temperature at the inlet to the fuel cell for a constant voltage.

4.6. Pressure drop of air flowing through the fuel cell as a function of the fuel cell operating voltage

Figure 8 shows a graph of the air pressure drop during flow through the fuel cell as a function of the fuel cell operating voltage for different values of temperature and velocity of air at the inlet to the fuel cell. Similarly to the case of the fuel, the air pressure drop during flow through the fuel cell increases with the increase of the cell operating voltage, which results, as previously described, from the decrease in the amount of reacted hydrogen per unit of the fuel cell surface and the model assumptions. Furthermore, three groups of curves for the assumed air velocities at the inlet to the fuel cell are clearly visible. The lowest values of the air pressure drop were obtained for the lowest air velocities at the inlet to the cell, and these values increase as the velocity increases. This results directly from Eq. (3), according to which the pressure drop during flow is proportional to the square of the flowing medium velocity. Moreover, for these three groups, a correlation can be observed between the increase in the air pressure drop as it flows through the fuel cell and the decrease in the air temperature at the inlet to the fuel cell. This dependence results from the decrease in the unit current intensity in the fuel cell with the decrease in the fuel cell temperature. The lower the unit current intensity, the lower the hydrogen utilisation. This affects the cell elongation, which in turn contributes to an increase in linear pressure losses. The relationship was described in detail in the previous paragraph.

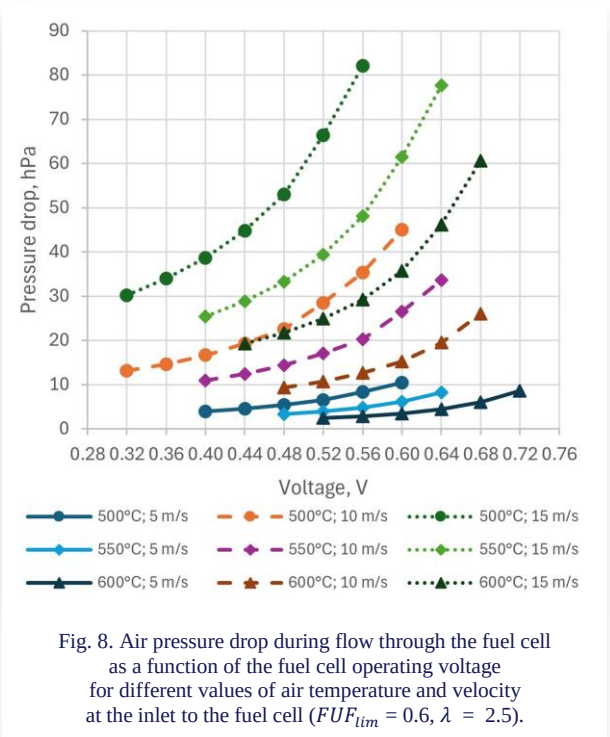

Fig. 8. Air pressure drop during flow through the fuel cell as a function of the fuel cell operating voltage for different values of air temperature and velocity at the inlet to the fuel cell (FUF_{lim} = 0.6, λ = 2.5).

4.7. Fuel cell electrical efficiency as a function of the excess air coefficient

Figure 9 shows a graph of the electrical efficiency of the fuel cell as a function of the excess air factor for different values of the cell operating voltage. The graph clearly shows that the excess air coefficient λ has no effect on the value of the electrical efficiency of the fuel cell, which in turn is strongly dependent on the value of the fuel cell operating voltage. It can be seen that with the increase in the cell operating voltage, the electrical efficiency of the fuel cell increases. The minimum value of over 13.5% is achieved for a voltage of 0.28 V, while the maximum value of about 31% is achieved for a voltage of 0.64 V.

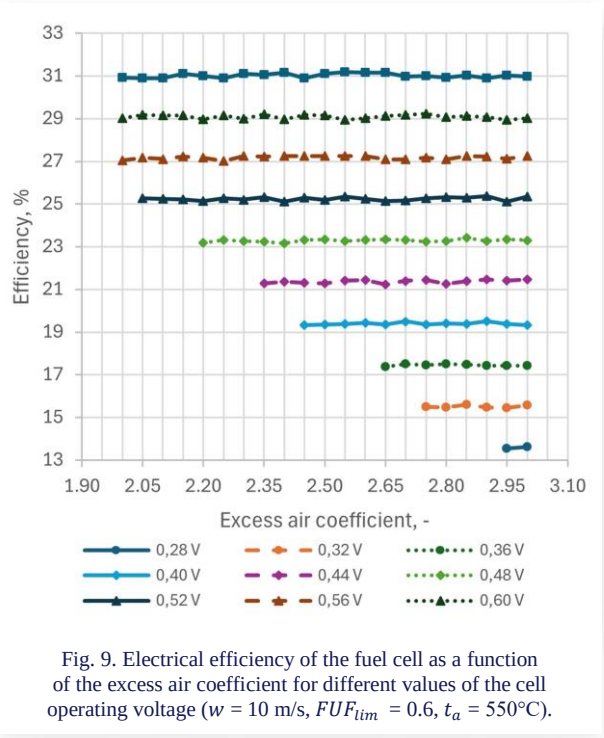

Fig. 9. Electrical efficiency of the fuel cell as a function of the excess air coefficient for different values of the cell operating voltage (w = 10 m/s, FUF_{lim} = 0.6, t_a = 550°C).

4.8. Electric power generated by the fuel cell as a function of the excess air coefficient

Figure 10 shows a plot of the electric power generated by the fuel cell as a function of the excess air coefficient for different values of the fuel cell operating voltage. Based on the graph, it can be concluded that the power of the fuel cell decreases as the

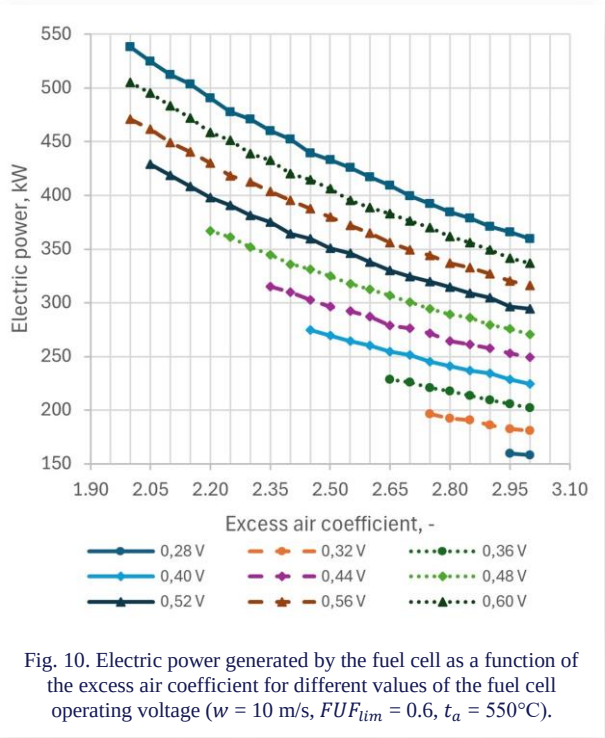

Fig. 10. Electric power generated by the fuel cell as a function of the excess air coefficient for different values of the fuel cell operating voltage (w = 10 m/s, FUF_{lim} = 0.6, t_a = 550°C).

excess air coefficient increases, which directly results from the calculation assumptions. The value of the air flow at the inlet to the fuel cell is a constant value, and for each case is 1 kg/s. In turn, the fuel flow is determined based on the excess air coefficient. With the increase of the excess air coefficient, the fuel flow supplied to the cell decreases, which directly results in a drop in the cell power output. Another relationship evident from the graph is that the cell power increases as its operating voltage increases. This results from the cell efficiency dependency on the cell operating voltage, which was discussed in the description of Fig. 9.

5. Conclusions

This paper presents a proposal for a 1D model of a solid oxide fuel cell. This model enables the determination of the fuel cell's operating range and key parameters, such as the power generated, surface area, length and operating temperature. It also calculates output parameters, including the temperature and pressure of the fuel and air at the cell's outlet. Additionally, the model assesses the variability of these values along the length of the cell.

Based on the conducted parametric analyses of the model, it was demonstrated that the proposed model accurately reflects the electro-physical properties of high-temperature fuel cells. Specifically, it was found that as the cell's operating voltage increases, its efficiency also increases; however, the unit fuel utilisation factor decreases. This decrease contributes to an increase in the fuel cell's surface area (cell elongation), which in turn affects the pressure drop of both air and fuel with the rise in voltage. Additionally, as voltage increases, the temperatures of the cell, air and fuel decrease. This phenomenon occurs because the amount of heat released by the cell diminishes due to the increase in electrical efficiency and the reduction in the unit fuel utilisation factor at higher voltages. Furthermore, as the temperature rises, the unit power of the fuel cell increases, which is directly related to the cell's current-voltage characteristics.

To ensure numerical robustness and physical validity, the model incorporates an error-handling routine that automatically discards input sets violating thermodynamic or electrochemical constraints. While this increases simulation reliability by eliminating unfeasible scenarios, it also narrows the output range and limits the model's ability to represent edge-case or transient operating conditions typical for advanced hybrid systems.

Despite its limitations, the model offers a computationally efficient and practical tool for early-stage solid oxide fuel cell design, including preliminary sizing, performance estimation and system-level techno-economic evaluation. Its implementation has already shown potential for use in conceptual design workflows, particularly in estimating operating conditions and supporting feasibility studies.

The primary limitation of the proposed model lies in its reliance on a specific current-voltage characteristic obtained from a fuel cell equipped with electrodes composed of a particular material. Consequently, to simulate a different type of fuel cell, the appropriate characteristic must be incorporated into the model. Future work will focus on extending the model by incorporating experimentally derived current-voltage characteristics for fuel cells utilising alternative electrode materials and operating under varied pressure conditions. This effort aims to build a database of diverse fuel cell configurations, thereby enhancing the model's versatility and broadening its applicability in system-level analyses.

Acknowledgements

The research was conducted as part of the implementation doctorate project, edition V, contract number RJO/SDW/005-14.

References

[1] Wang, J., Xu, Y., She, C., Xu, P., & Bagal, H.A. (2022). Optimal parameter identification of SOFC model using modified gray wolf optimization algorithm. *Energy*, 240, 122800. doi: 10.1016/j.energy.2021.122800

[2] www.energy.gov [accessed 12 Jan. 2024].

[3] Carrette, L., Friedrich, K.A., & Stimming, U. (2000). Fuel cells: principles, types, fuels, and applications. *ChemPhysChem*, 1(4), 162−193. doi: 10.1002/1439-7641(20001215)1:4<162::AID-CPHC162>3.0.CO;2-Z

[4] Faghri, A., & Guo, Z. (2005). Challenges and opportunities of thermal management issues related to fuel cell technology and modelling. *International Journal of Heat and Mass Transfer*, 48(19–20), 3891−3920. doi: 10.1016/j.ijheatmasstransfer.2005.04.014

[5] He, V., Gaffuri, M., Herle, J.V., & Schiffmann, J. (2023). Readiness evaluation of SOFC-MGT hybrid systems with carbon capture for distributed combined heat and power. *Energy Conversion and Management*, 278, 116728. doi: 10.1016/j.enconman.2023.116728

[6] Feng, Y., Qu, J., Zhu, Y., Wu, B., Wu, Y., Xiao, Z., & Liu, J. (2023). Progress and prospect of the novel integrated SOFC-ICE hybrid power system: System design, mass and heat integration, system optimization and techno-economic analysis. *Energy Con-*

version and Management: X, 18, 100350. doi: 10.1016/ j.ecmx. 2023.100350

[7] Alaedini, A.H., Tourani, H.K., & Saidi, M. (2023). A review of waste-to-hydrogen conversion technologies for solid oxide fuel cell (SOFC) applications: Aspect of gasification process and catalyst development. *Journal of Environmental Management*, 329, 117077. doi: 10.1016/j.jenvman.2022.117077

[8] Song, S., Xiong, X., Wu, X., & Xue, Z. (2021). Modeling the SOFC by BP neural network algorithm. *International Journal of Hydrogen Energy*, 46(38), 20065−20077, doi: 10.1016/ j.ijhydene.2021.03.132

[9] Barelli, L., Bidini, G., Cinti, G., & Ottaviano, P.A. (2022). Solid oxide fuel cell systems in hydrogen-based energy storage applications: Performance assessment in case of anode recirculation. *Journal of Energy Storage*, 54, 105257. doi: 10.1016/ j.est.2022. 105257

[10] Peters, R., Deja, R., Engelbracht, M., Frank, M., Nguyen, V.N., Blum, L., & Stolten, D. (2016). Efficiency analysis of a hydrogen-fueled solid oxide fuel cell system with anode off-gas recirculation. *Journal of Power Sources*, 328, 105−113. doi: 10.1016/ j.jpowsour.2016.08.002

[11] Marocco, P., Gandiglio, M., & Santarelli, M. (2022). When SOFC-based cogeneration systems become convenient? A cost-optimal analysis. *Energy Reports*, 8, 8709−8721. doi: 10.1016/ j.egyr.2022.06.015

[12] Baldi, F., Wang, L., Pérez-Fortes, M., & Maréchal, F. (2019). A cogeneration system based on solid oxide and proton exchange membrane fuel cells with hybrid storage for off-grid applications. *Frontiers in Energy Research*, 6, 139. doi: 10.3389/fenrg.2018. 00139

[13] Perdikaris, N., Panopoulos, K.D., Hofmann, Ph., Spyrakis, S., &, Kakaras, E. (2010). Design and exergetic analysis of a novel carbon free tri-generation system for hydrogen, power and heat production from natural gas, based on combined solid oxide fuel and electrolyser cells. *International Journal of Hydrogen Energy*, 35(6), 2446−2456. doi: 10.1016/j.ijhydene.2009.07.084

[14] Arsalis, A. (2019). A comprehensive review of fuel cell-based micro-combined-heat-and-power systems. *Renewable and Sustainable Energy Reviews*, 105, 391−414. doi: 10.1016/ j.rser.2019.02.013

[15] Wang, K., Hissel, D., Péra, M.C., Steiner, N., Marra, D., Sorrentino, M., Pianese, C., Monteverde, M., Cardone, P., & Saarinen, J. (2011). A Review on solid oxide fuel cell models. *International Journal of Hydrogen Energy*, 36(12), 7212−7228. doi: 10.1016/ j.ijhydene.2011.03.051

[16] Bove, R., & Ubertini, S. (2006). Modeling solid oxide fuel cell operation: Approaches, techniques and results. *Journal of Power Sources*, 159(1), 543−559. doi: 10.1016/j.jpowsour.2005.11.045

[17] Cheddie, D.F., & Munroe, N.D.H. (2007). A dynamic 1D model of a solid oxide fuel cell for real time simulation. *Journal of Power Sources*, 171(2), 634−643. doi: 10.1016/j.jpowsour.2007. 06.170

[18] Bharadwaj, A., Archer, D., & Rubin, E. (2005). Modeling the performance of a tubular solid oxide fuel cell. *Journal of Fuel Cell Science and Technology*, 2(1), 38−44. doi: 10.1115/1.1842781

[19] Karcz, M. (2009). From 0D to 1D modeling of tubular solid oxide fuel cell. *Energy Conversion and Management*, 50(9), 2307−2315. doi: 10.1016/j.enconman.2009.05.007

[20] Hajimolana, S.A., Hussain, M.A., Daud, W.M.A.W., Soroush, M., & Shamiri, A. (2011). Mathematical modeling of solid oxide fuel cells: A review. *Renewable and Sustainable Energy Reviews*, 15(4), 1893−1917. doi: 10.1016/j.rser.2010.12.011

[21] Calise, F., Dentice d'Accadia, M., Palombo, A., & Vanoli, L. (2008). One-dimensional model of a tubular solid oxide fuel cell. *Journal of Fuel Cell Science and Technology*, 5(2), 021014. doi: 10.1115/1.2784296

[22] Min, G., Park, Y.J., & Hong, J. (2020). 1D thermodynamic modeling for a solid oxide fuel cell stack and parametric study for its optimal operating conditions. *Energy Conversion and Management*, 209, 112614. doi: 10.1016/j.enconman.2020.112614

[23] Luo, X.J., & Fong, K.F. (2016). Development of 2D dynamic model for hydrogen-fed and methane-fed solid oxide fuel cells. *Journal of Power Sources*, 328, 91−104. doi: 10.1016/j.jpowsour. 2016.08.005

[24] Conti, B., Bosio, B., McPhail, S.J., Santoni, F., Pumiglia, D., & Arato, E. (2019). A 2-D model for intermediate temperature solid oxide fuel cells preliminarily validated on local values. *Catalysts*, 9(1), 36. doi: 10.3390/catal9010036

[25] Ferguson, J.R., Fiard, J.M., & Herbin, R. (1996). Three-dimensional numerical simulation for various geometries of solid oxide fuel cells. *Journal of Power Sources*, 58(2), 109−122. doi: 10.1016/0378-7753(95)02269-4

[26] Al-Masri, A., Peksen, M., Blum, L., & Stolten, D. (2014). A 3D CFD model for predicting the temperature distribution in a full scale APU SOFC short stack under transient operating conditions. *Applied Energy*, 135, 539−547. doi: 10.1016/j.apenergy. 2014.08.052

[27] Xiong,. X., Liang, K., Ma, G., & Ba, L. (2023). Three-dimensional multi-physics modeling and structural optimization of SOFC large-scale stack and stack tower. *International Journal of Hydrogen Energy*, 48(7), 2742−2761. doi: 10.1016/ j.ijhydene. 2022.10.146

[28] Kim, D.H., Bae, Y., Lee, S., Son, J.-W., Shim, J.H., & Hong, J. (2020). Thermal analysis of a 1-kW hydrogen-fueled solid oxide fuel cell stack by three-dimensional numerical simulation. *Energy Conversion and Management*, 222, 113213. doi: 10.1016/ j.enconman.2020.113213

[29] Milewski, J. (2012). A *Mathematical Model* of SOFC: A proposal. *Fuel cells*, 12(5), 709−721. doi: 10.1002/fuce.201100150

[30] dos Santos-Gómez, L., Zamudio-García, J., Porras-Vázquez, J.M., Losilla, E.R., & Marrero-López, D. (2018). Highly efficient $La_{0.8}Sr_{0.2}MnO_{3-\delta}$ - $Ce_{0.9Gd0.1}O_{1.95}$ nanocomposite cathodes for solid oxide fuel cells. *Ceramics International*, 44(5), 4961−4966. doi: 10.1016/j.ceramint.2017.12.089

[31] Esposito, V., Gadea, Ch., Hjelm, J., Marani, D., Hu, O., Agersted, K., Ramousse, S., & Jensen, S.H. (2015). Fabrication of thin yttria-stabilized-zirconia dense electrolyte layers by inkjet printing for high performing solid oxide fuel cells. *Journal of Power Sources*, 273, 89−95. doi: 10.1016/j.jpowsour.2014.09.085

[32] Shimada, H., Yamaguchi, T., Sumi, H., Nomura, K., Yamaguchi, Y., & Fujishiro, Y. (2017). Extremely fine structured cathode for solid oxide fuel cells using Sr-doped $LaMnO_3$ and Y_2O_3-stabilized ZrO_2 nano-composite powder synthesized by spray pyrolysis. *Journal of Power Sources*, 341, 280−284. doi: 10.1016/ j.jpowsour.2016.12.002

[33] Shimada, H., Sumi, H., Yamaguchi, Y., Nomura, K., Mizutani, Y., Fujishiro, Y., & Shin, W. (2023). Boosting power density of solid oxide fuel cells by synergistic effect of nanocomposite cathode and anode. *Journal of Power Sources*, 563, 232781. doi: 10.1016/j.jpowsour.2023.232781

[34] Churchill, S.W. (1973). Empirical expressions for the shear stress in turbulent flow in commercial pipe. *American Institute of Chemical Engineers Journal*, 19(2), 375−376. doi: 10.1002/aic. 690190228

[35] http://www.coolprop.org/ [accessed 12 Jan. 2024].

[36] Klemes, J.J., Arsenyeva, O., Kapustenko, P., & Tovazhnyanskyy, L. (2017). *Compact heat exchangers for energy transfer intensification − low grade heat and fouling mitigation*. CRC Press.